

A volcano curve: optimizing methanol electro-oxidation on Pt-decorated Ru nanoparticles†

Bingchen Du,^a Savelas A. Rabb,^b Christopher Zangmeister^b and YuYe Tong^{*a}

Received 22nd September 2008, Accepted 26th May 2009

First published as an Advance Article on the web 26th June 2009

DOI: 10.1039/b816531a

Controlled Pt adlayers were deposited on commercial Ru nanoparticles (NPs) using an industrially scalable one-pot ethylene glycol (EG) reduction based method and were characterized by X-ray diffraction (XRD), electrochemical (EC) CO stripping voltammetry, inductively-coupled plasma optical emission spectrometry (ICP-OES), X-ray photoemission spectroscopy (XPS), and transmission electron microscopy (TEM). Compared with the previously used “spontaneous deposition”, the wet chemistry-based EG method is less technically demanding, *i.e.* no need to handle high-temperature hydrogen reduction, offers a better control of the Pt packing density (PD), enables the formation of stable, segregated Pt surface adlayers for optimal tuning and use of Pt, and effectively prevents NPs sintering. Two batches of a total of 11 (8 *vs.* 3) samples with different values of Pt PD ranging from 0.05 to 0.93 were prepared, with a time interval of more than 18 months between the syntheses of the two batches of samples, and an excellent reproducibility of results was observed. All samples were investigated in terms of methanol (MeOH) electro-oxidation (EO) by cyclic voltammetry (CV) and chronoamperometry (CA). Although the peak current of CV increased as the Pt content increased, the long-term steady-state MeOH electro-oxidation current density of the Pt-decorated Ru NPs measured by CA showed a volcano curve as a function of the Pt PD, with the maximum appearing at the PD of 0.31. The optimal peak activity was $\sim 150\%$ higher than that of the industrial benchmark PtRu (1 : 1) alloy NPs and could deliver the same performance at half the electrode material cost. Fundamentally, such a volcano curve in the reaction current is the result of two competing processes of the EO of MeOH: the triple dehydrogenation of MeOH that prefers more Pt ensemble sites, and the elimination of poisonous CO that is enhanced by more adjacent Ru/Pt sites *via* the so-called bifunctional mechanism and also by possible electronic effects at low Pt coverages.

1. Introduction

Pt has long been used as the major component of anode electrocatalysts for electro-oxidation (EO) of methanol (MeOH) in direct MeOH fuel cells (DMFCs).¹ However, two major, long outstanding obstacles still exist that prevent large scale practical applications of the DMFC. One is the CO poisoning during the EO of MeOH, which quickly lowers the catalytic activity of Pt. The other is the high loading of Pt needed in the anode to sustain the performance, which noticeably increases the cost of the whole fuel cell system. Numerous efforts have been made both to improve the CO tolerance and to reduce Pt loading.^{2,3} For both purposes, binary or ternary Pt-based metallic/metal oxide catalysts, such as PtRu,⁴ PtNi,⁵ PtSn,⁶ and PtRuTiO₂⁷ have been studied, among which, the PtRu alloy has been shown to have the best

practical performance.^{8,9} Consequently, most of the recent research in this field has focused on manipulating PtRu from different perspectives, such as varying the molar ratio between Pt and Ru,¹⁰ improving synthetic methods,^{11,12} and adopting different carbon supporting materials.^{13–15} Recently, Brankovic *et al.*¹⁶ adopted a spontaneous deposition method (that was first used in reverse; depositing Ru on single crystal Pt surfaces¹⁷) to decorate the surface of carbon-supported Ru NPs with Pt. The method involved a necessary step of reducing Ru NPs with hydrogen gas at relatively high temperature (300 °C). The resulting NPs, according to that work, offered the advantage of maintaining the activity towards CO tolerance with a much reduced Pt loading of ~ 10 wt% compared to commercially available E-TEK PtRu (1 : 1) which has a Pt loading of ~ 66 wt%. Later on, Kuk and Wieckowski¹⁸ also applied a similar method to cover Ru and carbon-supported Ru NPs with different Pt loading using repetitive hydrogen reduction and spontaneous depositions. While the Pt packing densities (PDs) were determined using inductively-coupled plasma mass spectrometry (ICP-MS), the analysis of the true surface coverage and the associated activity was complicated by the possibility of Pt penetrating into Ru NPs and the observed sintering effect due to high temperature reduction.

^a Department of Chemistry, Georgetown University, 37th & O Streets, NW, Washington DC, 20057, USA. E-mail: yyt@georgetown.edu

^b Chemical Science and Technology Lab, National Institute of Standards and Technology, 100 Bureau Drive, Gaithersburg, MD, 20899, USA

† Electronic supplementary information (ESI) available: CV and XPS spectra, TEM images and CA curves of 2nd batch samples. See DOI: 10.1039/b816531a

Although this spontaneous deposition method opens up a promising way of fabricating anode materials of low Pt loading, handling high temperature hydrogen reduction is technically less appealing, and repetitive hydrogen reduction and spontaneous depositions are often tedious and struggle to achieve quantitative control of the Pt coverage. Furthermore, the procedure would be difficult to implement on a large industrial scale.

In an attempt to address the technically important controllability of the Pt PD and the scalability of the operation, we have developed a superior, industrially scalable ethylene glycol (EG) reduction based wet chemistry method that allowed us to achieve a quantitative control of the Pt PD on Ru NPs and optimize the activity of the EO of MeOH. It started with commercially available Ru NPs (~ 3 nm). Pt salt was then reduced using the mild reducing power of EG to cover the Ru NPs. Careful electrochemical (EC) measurements showed that by varying the Pt:Ru molar ratio of the starting materials, the EG method enabled a relatively easy control of the Pt PD that followed the nominal Pt:Ru molar ratio linearly. ICP optical emission spectrometry (ICP-OES) and X-ray photoemission (XPS) measurements were carried out on three of the second batch samples and gave consistent Pt PDs as determined by the EC method. Detailed transmission electron microscopy (TEM) measurements on these three samples showed very similar particle size distributions and no evidence of pure Pt NP formation. Powder X-ray diffraction (XRD) measurements were carried out on two representative samples of the first batch and three samples of the second batch. These results indicated that the samples were neither pure Ru, Pt, nor PtRu alloy, consistent with the formation of Pt adlayers on Ru NPs. Furthermore, the as-prepared Pt-decorated Ru NPs displayed revealing Pt PD-dependent EC characteristics in CO stripping and MeOH EO. In particular, a volcano curve, peaking at a Pt PD of 0.31 in long-term steady-state MeOH activity as gauged by chronoamperometric (CA) current measured at 60 min and 0.2 V (with respect to the Ag/AgCl (3M) reference electrode), was observed. The peak activity was $\sim 150\%$ higher than that of the industrial benchmark PtRu (1:1) alloy NPs.¹⁹ Technologically, with the higher activity achieved, and lower Pt loading, one could expect at least a 50% decrease in catalytic material cost. Fundamentally, the observation of the volcano curve as a function of the Pt coverage can be largely rationalized by the so-called “bifunctional mechanism”²⁰ in which the electro-oxidation of the poisonous CO intermediate preferentially adsorbed at Pt sites occurs at a lower potential due to the supply of oxygen-containing species formed at the adjacent Ru sites.

2. Experimental

2.1 Preparation of the Pt-decorated Ru NPs

All commercial high-surface area Ru, PtRu (1:1) alloy, and Pt NPs used either as the starting material or references in this study were courtesy of Johnson–Matthey.

It has been experimentally confirmed that, when in contact with air, Ru NPs are readily oxidized to form RuO_x.^{21,22} Our

previously published data,²³ and those of others,²⁴ have reported that the presence of RuO_x makes it difficult to deposit Pt onto the surface of Ru NPs. Thus, the first step is to completely reduce the Ru surface. Previous studies^{16,18} employed hydrogen gas reduction, usually at relatively high temperature (200 to 300 °C), to reduce the Ru surface. In order to vary the Pt coverage, tedious, repetitive hydrogen reduction and spontaneous deposition cycles were employed, which could easily cause unwanted penetration of Pt into the Ru NPs and electrocatalyst sintering.¹⁸ Consequently, it becomes very challenging to control and tune the Pt PD. That is, the Pt PD is not known *a priori*. It would also be quite difficult to scale up this procedure for potential industrial applications.

Here, we describe a wet chemistry based, homogeneous reaction-like procedure using EG as both reaction medium and reductant for the reduction of Ru NPs and the subsequent deposition of Pt. This new approach is advantageous in two respects. One is that the homogeneous-reaction-like medium is better at preventing sintering (*vide infra*) and is, in principle, industrially scalable. The other is that the mild reducing power of EG offers better control of Pt deposition on Ru NPs. Specifically, the samples studied in this paper were prepared as follows: 5 mg of the 3 nm Johnson–Matthey (J–M) Ru NPs was dispersed ultrasonically into EG to form a homogeneous ink, which was heated at 140 °C for 2 h with vigorous stirring to reduce oxide species on the Ru surface. The efficiency of this reduction step is clearly demonstrated by comparing the corresponding CVs of the Ru NPs as shown in Fig. 1. According to Brankovic *et al.*,²⁵ the large cathodic peak at around -0.2 V in the CV of the cleaned Ru NPs (Fig. 1B) was due to the adsorption of oxygen-containing species, *e.g.* OH groups, and could be considered a hallmark of well reduced Ru NPs. Notice that this cathodic peak was largely absent for the as-received Ru NPs because the surface had already been covered by RuO_x. Green *et al.*,²⁶ however, attributed this peak to a co-adsorption of hydrogen and oxygen-containing species. In any case, the contributions from the adsorption of oxygen-containing species distinguish Ru from Pt and Pd in that the latter adsorb only hydrogen in this potential region.

The cleaned J–M Ru NPs were then collected and rinsed with ethanol and re-dispersed ultrasonically into a fresh EG solution with the calculated volume of H₂PtCl₆ solution that gave the desired nominal Pt:Ru molar ratio. After a 30 min long ultrasonication, the mixture was heated at 120 °C for 4 h to reduce Pt(IV) to Pt(0) on the surface of the J–M Ru NPs. The final product was collected and rinsed several times with ethanol. The first prepared batch consisted of eight samples

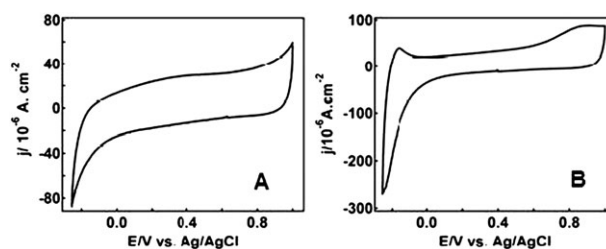


Fig. 1 Comparison of the CVs of (A) the as-received Ru NPs and (B) the EG-cleaned Ru NPs.

with nominal Pt:Ru molar ratios of 1:20, 1:10, 1:6, 1:5, 1:4, 1:3, 1:2, and 1:1.5, respectively and the second batch of three samples with nominal Pt:Ru molar ratios of 1:13.3, 1:4, and 1:2.7, respectively, with an interval of more than 18 months between them. It was found that the degrees of dispersiveness of the starting Ru NPs and their reductive cleanness were critically important to obtaining good reproducibility.

2.2 Electrochemistry

The working electrode was prepared as follows. The as-prepared Pt-decorated Ru NPs were transferred into a mixed solution of 2-propanol and 5 wt% Nafion[®] (Du Pont, Inc) solution. It was found that the following ratio of the above ingredients gave the optimum EC results: 1 mg PtRu sample, 0.2 ml 2-propanol, 1 μ l Nafion solution. The mixture was then ultrasonicated for at least 10 min to form a uniform suspension which was drop-cast onto the surface of a commercial (Bioanalytical) 3 mm-diameter glassy carbon (GC) electrode. The electrode surface was air dried under a gentle Ar flow and rinsed with a copious amount of Milli-Q water (18.2 M Ω cm) to eliminate loosely attached NPs.

All EC experiments were carried out in an Ar-blanketed, conventional three-electrode EC cell using an EG&G273A potentiostat (Princeton Applied Research) controlled by a PC with the CoreWare software package (Scribner). All CVs were recorded with a scan rate of 50 mV s⁻¹. The commercial GC electrode, Pt gauze and Ag/AgCl (3M) (Bioanalytical) were used as working, counter, and reference electrodes, respectively. All electrode potentials in this paper were cited with respect to the Ag/AgCl (3M) reference electrode (0.290 V with respect to RHE) and all current densities were calculated using the total surface area as determined by the CO stripping peak. A 0.1M HClO₄ solution prepared with Milli-Q water was used as the electrolyte. For CO stripping experiments, ultrahigh purity CO gas (MG Industries) was bubbled for 2 min followed by Ar bubbling for another 5 min. During the whole process, potential was held at 0 V. At least two cycles of CVs were recorded to make sure that all of the CO molecules oxidized were from the electrode surface, not from the residual CO in the electrolyte solution. For EO of MeOH, a 0.1 M HClO₄ solution with 0.5 M MeOH was used. In the CA experiments which were run first, the electrode was pre-cleaned by holding the potential at 0 V until the current decayed to a negligible level, and then the MeOH was injected under an active stirring condition. The CA curves were recorded while the potential was held at 0.2 V for 1 h. Under the same conditions, the background current was measured without the presence of MeOH and was subtracted from the CA curve. After the CA measurements, multiple cycles were run to obtain the stable and repeatable EO of MeOH CVs that are shown in the paper.

2.3 XRD, TEM, XPS, and ICP-OES

XRD measurements were carried out using a Rigaku RAPID curved IP X-ray powder diffractometer with Cu K α radiation (1.5406 Å) and an image plate detector. For XRD sample preparation, the as-prepared samples were completely dried in

a vacuum desiccator and then transferred into a 0.5 mm diameter sample tube (Mark-Rohrchen) which was ready for measurement use after flame-sealing.

TEM samples were prepared by depositing diluted NP suspensions onto carbon-coated copper grids. The images were taken on a JOEL JEM-2100 FE-TEM at the Nanoscale Imaging Spectroscopy and Properties Lab, University of Maryland.

XP spectral data were acquired on a Kratos Axis Ultra DLD using an Al K α (1486.7 eV) source. Samples were drop-cast from sonicated methanol suspensions onto cleaned Si substrates. Experiments were run on two different spots of the same substrate to ensure the consistency of the measurements.

ICP-OES measurements were conducted in the axial mode using a PerkinElmer Optima 5300 DV ICP-OES instrument. Operating conditions were as follows: power = 1.5 kW; nebulizer gas flow = 0.6 L min⁻¹; auxiliary gas flow = 0.5 L min⁻¹; sample uptake = 1 mL min⁻¹. A MiraMist nebulizer and cyclonic spray chamber were used to introduce the samples into the ICP. The calibration was performed by using the method of standard additions to compensate for any matrix effects. Pt 265.945 and Ru 240.272 were observed to determine the Pt and Ru sample concentrations with Sc 357.634 as an internal standard emission line. Three to four different aliquots were prepared for each sample and two measurements were performed on each aliquot. The average of these measurements is reported. As a control, the Johnson–Matthey PtRu (1:1) alloy NPs sample was analyzed with the Pt-decorated samples in two independent runs. The averaged results of the Pt:Ru ratio from the alloy sample were 1.14 \pm 0.03 and 1.10 \pm 0.06, respectively.

3. Results and discussions

3.1 Pt packing density (PD): the formation of segregated atomic adlayers

The state of the Pt deposited on the Ru NP surface needs to be addressed first. Technically, it is still a challenge to determine the fraction of Pt surface area in Pt-based bimetallic, particularly Pt–Ru, NPs. For pure Pt, the electrochemically active surface area of Pt has been routinely determined by using the charge associated with hydrogen desorption,²⁷ CO stripping,²⁸ or Pt oxide reduction.^{23,29} The former two methods, however, may produce large uncertainty if used for Pt–Ru bimetallic surface due, respectively, to the interference of the adsorption/desorption of oxygen-containing species (see Fig. 1B) and the indiscriminate nature of CO adsorption with respect to the Pt and Ru sites. We therefore adopted a method that combines the CO stripping and Pt oxide reduction. Because of the indiscriminate nature of CO adsorption, CO stripping with a well-known reaction stoichiometry (2e per CO oxidation and the charge density of 420 μ C cm⁻² was used for calculating the surface area) provides a good and straightforward estimate of the total surface area accessible to CO adsorption. On the other hand, using Pt oxide reduction charge to determine the Pt surface area is more complicated because the reaction stoichiometry is not as well defined as the CO oxidation.²⁸ However, it can still offer a reasonable estimate of the Pt surface area,²³ particularly

when the corresponding charge density is reasonably well calibrated by a known quantity. Here, we used the J–M Pt NPs as the reference in which the Pt oxide reduction charge was calibrated by the CO stripping charge (see the dashed CV in Fig. 2(h)). This gave a charge density of $400 \mu\text{C cm}^{-2}$ that we used to calculate the Pt surface area (notice that this charge density value is very close to the one obtained by Kozłowska *et al.*³⁰). The Pt PD was then calculated by the ratio between the surface area determined by the Pt oxide reduction, which was Pt specific, and that determined by the CO stripping.

Fig. 2 shows the CO stripping CVs of the eight samples of the first prepared sample batch. The dashed CVs in Fig. 2(a), (f), and (h) are those of the J–M Ru (the starting material), J–M PtRu (1 : 1) alloy, and pure J–M Pt NPs, respectively, used as references for the purpose of comparison. Reproducible results were obtained on the three samples of the second batch as shown in Fig. S1 in the ESI†. Using these data, the Pt PDs were calculated by the approach described above and the values obtained are listed in Table 1. For the purpose of comparison, the values of the nominal PD calculated using the nominal Pt:Ru molar ratios are also listed. Here, we assumed that all the Pt(IV) were reduced to Pt(0) on the metallic Ru surface sites that acted as nucleation centers for the Pt deposition²³ and then formed adlayers of mono-atomic height. Taking an average size of 3 nm (see the TEM results below), the dispersion of the J–M Ru NPs was estimated

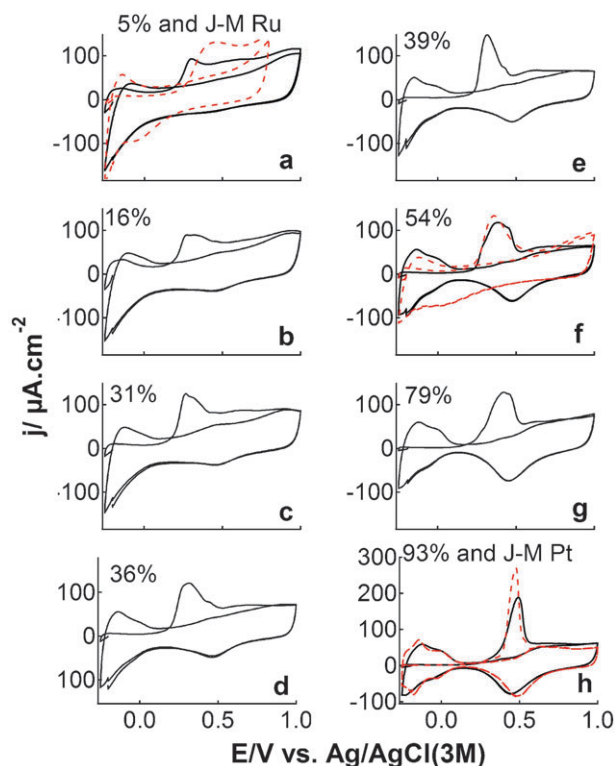


Fig. 2 The CO stripping CVs and, thereafter, those of the eight Pt-decorated Ru NP samples of the first batch. The dashed CVs in (a), (f), and (h) are those of pure J–M Ru, J–M PtRu (1 : 1) alloy, and J–M pure Pt NPs that are used as references for comparison. The percentage numbers are the values of Pt PD calculated by the method described in the text. Reproducible results were obtained on the three samples of the second batch as shown in Fig. S1 of the ESI†.

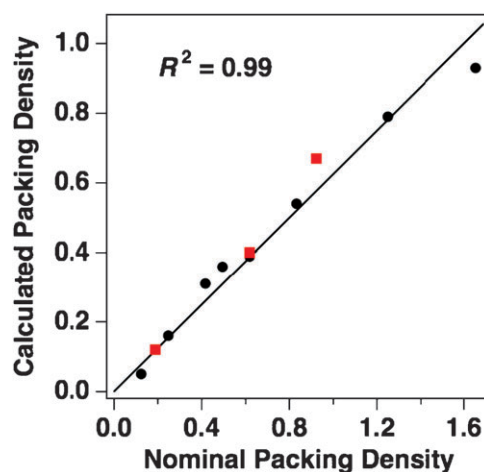


Fig. 3 The linear relationship between the measured and the nominal Pt packing density (PD). Squares are for the three, 2nd batch samples. The straight line goes through the origin.

to be $\sim 40\%$ according to the Benfield's calculation.³¹ Thus, the values of the nominal Pt PD were then calculated by equation: $\text{PD} = \text{Pt:Ru molar ratio}/0.40$. Notice that the values of the Pt PD as determined by the charges of Pt oxide reduction and CO stripping, although being constantly lower than the respective nominal ones (likely due to the value of $400 \mu\text{C}/\text{cm}^2$ overestimating the charge density for Pt oxide reduction on Ru surface (a value of $250 \mu\text{C}/\text{cm}^2$ would give a slope of 1) and/or to 3D packing), followed the trend of the nominal PD linearly ($y = ax$ with $R^2 = 0.99$, Fig. 3), therefore enabling a quantitative control of the Pt PD in one-pot synthesis. The squares in Fig. 3 are from the three samples of the second batch, demonstrating excellent reproducibility.

The Pt PDs determined by ICP-OES for the three samples of the second batch are, respectively, 0.36, 0.66 and 0.86, which are in a good agreement with the nominal Pt PDs shown in Table 1. For the XPS measurements on the same samples, the Ru NP diameter (*ca.* 3 nm) is $> 2\times$ the inelastic mean free path (IMFP, see below), thus modeling these systems as a 2-dimensional Ru surface was used. The attenuation of photoemission from the Ru core by the Pt overlayer was accounted for using the NIST standard reference database 82 (NIST Electron Effective Attenuation Length Database, Ver. 1.1) using an IMFP of 1.329 nm at 462 eV (Ru 3d binding energy, 1025 eV kinetic energy). The Ru 3d intensity was compared to the Pt 4d and 4f. Representative XP spectra are shown in Fig. S2 in the ESI†. Assuming a 0.7 nm Pt overlayer thickness (0.27 attenuation factor) and neglecting any other surface adsorbed species, the model analysis gave the Pt PD values as 0.55, 0.72 and 1.35, respectively. If an additional 0.5 nm carbon overlayer was used to model the ubiquitous surface adsorption, the corresponding PD values became 0.31, 0.40 and 0.79, respectively, in reasonable agreement with the values shown in Table 1. The fact that such high Pt contents were obtained from the XPS data without using the Ru core–Pt shell structure suggested that what we had synthesized were indeed Ru@Pt NPs.

Finally, for facilitating the following discussions, the as-prepared Pt-decorated Ru samples are named as Pt(EC-measured PD)–Ru, *e.g.* Pt(16)–Ru = 16% Pt-decorated Ru.

Table 1 Comparison of the nominal and measured Pt packing densities (* indicates the 2nd sample batch)

Pt:Ru ratio	1:20	1:13.3*	1:10	1:6	1:5	1:4	1:3	1:2.7*	1:2	1:1.5
Nominal PD	0.12	0.19	0.25	0.42	0.50	0.62	0.83	0.92	1.25	1.65
Measured PD	0.05	0.12	0.16	0.31	0.36	0.39 (0.40*)	0.54	0.67	0.79	0.93

Another important question that needs to be addressed convincingly is whether the Pt ended up on Ru NP surface or formed pure Pt NPs. For this purpose, we carried out detailed TEM and XRD measurements on the three samples of the second batch and on the starting Ru NPs. We also obtained XRD measurements of two representative samples of the first batch (Pt(31)-Ru and Pt(93)-Ru). The average particle sizes measured (with ~ 150 counts for each sample) by TEM are 3.1 ± 0.4 nm, 3.1 ± 0.3 nm, 3.2 ± 0.3 nm and 3.0 ± 0.4 nm for pure Ru NPs, Pt(12)-Ru, Pt(40)-Ru, and Pt(67)-Ru, respectively. From these TEM data, it is clear that no sintering of the NPs happened and that the Pt shell was predominantly of mono-atomic height. Fig. 4(a) and (b) compare the representative TEM images of the pure Ru and Pt(67)-Ru (see Fig. S3 in the ESI† for the TEM images of Pt(12)-Ru and Pt(40)-Ru). The insets are the corresponding high resolution TEM (HRTEM) images. By measuring, almost exhaustively, the distances between adjacent atomic planes as revealed by the HRTEM images (insets in Fig. 4(a) and (b)),

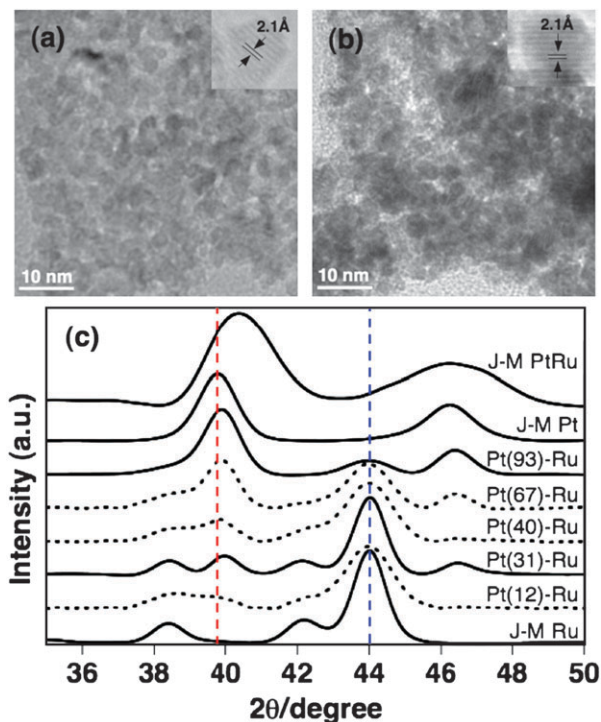


Fig. 4 The TEM images of (a) the starting Ru NPs and (b) Pt(67)-Ru. The insets are the corresponding HRTEM snapshots where the distance between two adjacent atomic planes was measured to be 0.21 nm for both samples. (c) XRD patterns within the small angle range for two representative Pt-decorated Ru samples of the 1st batch and for the three samples of the 2nd batch. Those for pure J-M Pt, J-M PtRu alloy, and pure Ru NPs are also shown for comparison. The vertical dashed lines indicate the respective standard angle positions of Pt(111) (left) and Ru(101) (right) as references.

no evidence of Pt NP formation was found: all measured distances were about 0.21 nm (Fig. 4(b)), the same as that measured on pure Ru NPs (Fig. 4(a)).

The results of XRD are shown in Fig. 4(c) together with those of the pure J-M Pt, J-M PtRu (1:1) alloy, and the pure starting J-M Ru NPs for comparisons. The XRD of the J-M Pt and Ru NPs reproduced all standard peak positions of which the main peaks within the angle range are located at $38.38^\circ(100)$, $42.15^\circ(002)$, $44.00^\circ(101)$ for Ru (PDF#06-0663) and at $39.76^\circ(111)$, $46.24^\circ(200)$ for Pt (PDF#04-0802). The vertical dashed lines in Fig. 4(c) indicate the respective standard positions of Pt(111) (left) and Ru(101) (right) as references.

As can be seen in Fig. 4(c), the Ru(101) peak amplitude decreases gradually but the peak position remains the same as the Pt PD increases. These are strong indications showing that the Ru NPs were gradually covered by Pt and no PtRu alloy was formed. At the same time, a growing peak corresponding to Pt appears with a peak position slightly larger than, but not exactly at, that of Pt(111). Using the Bragg's law $\lambda = 2d \sin \theta$, the d corresponding to the Pt(93)-Ru peak ($2\theta = 39.91^\circ$) is 0.2256 nm. This value is very close to the height (0.2248 nm) of a Pt atom sitting in a close-packed fashion at a three-fold site of a Ru(0001) surface. Because of the mismatch of the close-packed atomic distances between Pt (0.2772 nm) and Ru (0.2701 nm), the height of a pseudo-morphic growth of a Pt(111) monolayer on a Ru(0001) surface is expected to be larger than 0.2248 nm. On the other hand, the d of a close-packed Pt(111) plane is 0.2265 nm. Therefore, the d value of 0.2256 nm strongly suggests that the Pt adlayers formed were predominantly of mono-atomic height. The growth of the peak intensity indicated that the Ru surface was covered more and more by Pt adlayers. Similar intensity was also reported recently for the synthesized Ru@Pt NPs with 1 to 2 Pt atomic layers.³² Such Ru@Pt structure was further corroborated by the strong dissimilarity between the XRD pattern of Pt(93)-Ru and that of J-M PtRu alloy NPs^{33,34} that largely eliminates any major formation of alloy in Pt(93)-Ru.

The formation and growth of the Pt adlayer on the Ru NP surface are further corroborated by the EC data shown in Fig. 2. For all the coverage values, no separate peak, expected for pure Pt NPs, was observed,³⁵ indicating that few, if any, pure Pt NPs were formed during the Pt deposition. For Pt(5)-Ru (Fig. 2a), two features in the CO stripping CV are worth highlighting: one is the appearance of a narrower and small peak that was negatively shifted by as much as 0.17 V with respect to the broader CO stripping peak observed on the pure J-M Ru NPs (dashed CV in Fig. 2a). This may be a direct manifestation of the bifunctional mechanism well-articulated for a Pt-Ru surface^{36,37} as well as a possible additional electronic (ligand and strain) effect,³⁸⁻⁴⁰ thus indicating a direct deposition of Pt on Ru. The other is the broad shoulder at the high potential that is different from that of the pure J-M

Ru NPs but can be reasonably assigned to the CO oxidation at the Ru sites distant from the deposited Pt sites. As the Pt PD increased, the low-potential Pt–Ru peak grew larger at the expense of the broader high-potential Ru peak. These gradual and monotonic changes strongly suggest that the Pt went onto the Ru surface forming nanosize Pt islands instead of forming pure Pt NPs, which is very similar to cases of Ru-decorated Pt NPs.⁴¹

An intriguing observation is that, in great contrast to the PtRu alloy NPs in which no well-defined Pt oxide reduction peak was observed (see dashed CV in Fig. 2(f)), the 11 Pt-decorated Ru NP samples studied here all showed well defined Pt oxide reduction peaks that enabled the Pt surface area to be determined. This observation attests that no PtRu alloy was formed, but, rather, a segregated Pt adlayer on the Ru surface. Additionally, the monotonic decrease in the double-layer current as the Pt coverage increased also indicates that the Ru surface was gradually covered up by the Pt. Similar observations on Ru-decorated Pt NPs were made previously^{19,42,43} in that, for Ru-decorated Pt NPs, the deposition of Ru was accompanied by an increase in the double-layer capacitance, a decrease in the hydrogen adsorption area and a change in the oxide stripping peak.⁴¹ Notice that large double-layer capacitance of the characteristics of pure Ru NPs would show up if physically separated Pt and Ru NPs did exist.^{35,44} But it is clearly not the case here. In summary, the above observations made from several independent perspectives all together provide a convincing convergence that is consistent with the formation of Pt adlayers on Ru NPs surface.

The variations in the shape and potential of the CO stripping peak as a function of Pt PD are highly revealing (the latter is shown in Fig. 5a). As the Pt PD increased, it started with a large (~ 0.17 V) negative shift that peaked at the Pt PD of 0.31. (However, the shift is less negative than that observed on the Ru-decorated Pt NPs.^{19,39}) At the same time, it shows a fast rising front and a slow decreasing back, indicating a dominant electro-oxidation of CO at the peripheral Ru/Pt sites.⁴¹ The peak then moved

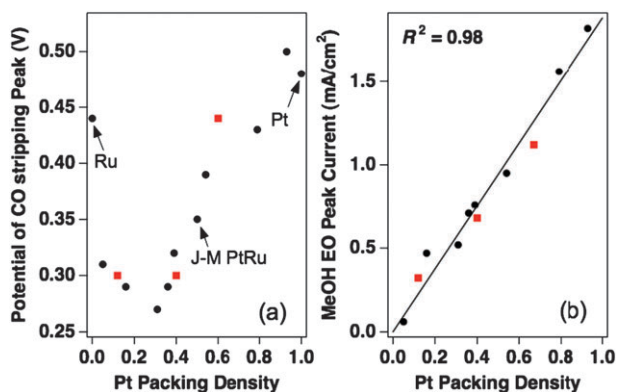


Fig. 5 (a) The Pt coverage dependence of the CO stripping peak potentials. The CO stripping peak potentials of the pure J–M Ru, J–M PtRu (1 : 1) alloy, and J–M Pt NPs (as labeled) are also shown in the figure for comparison. (b) A linear relationship between the MeOH EO peak current and the Pt PD. The straight line goes through the origin. The squares are of the three samples of the 2nd batch.

positively in the opposite direction until the potential value of the pure Pt NPs was recovered at the Pt PD of 0.93, accompanied by a change to a slow rising front and a fast decreasing back which indicates a dominant EO of CO on Pt terrace sites, in agreement with a fully Pt covered Ru surface. Indeed, the latter sample showed characteristics almost identical to those of the pure Pt NPs (Fig. 2(h) and *vide infra*). It is also interesting to point out that, although the Pt(54)–Ru and the J–M PtRu (1 : 1) alloy NPs showed very similar CO stripping peaks, their overall CVs were arguably dissimilar (Fig. 2(f)), implying different surface structure, electronic properties and catalytic behaviors. Most importantly, the pattern shown in Fig. 5(a) strongly suggests that, for the Pt adlayer–Ru substrate systems studied here, the bifunctional mechanism was the dominant force in achieving the enhanced CO-eliminating ability and the active sites were highly likely to exist along the peripheries of the Pt adlayers, similar to the cases of Ru-decorated Pt surfaces.^{45,46} On the other hand, although the electronic effects of the Ru substrate on the Pt adlayers might play a stronger synergistic role at the lower Pt PDs,^{38,39} it would become smaller and smaller as evidenced by the recovering of the characteristics of the pure Pt surface towards the high Pt coverage.

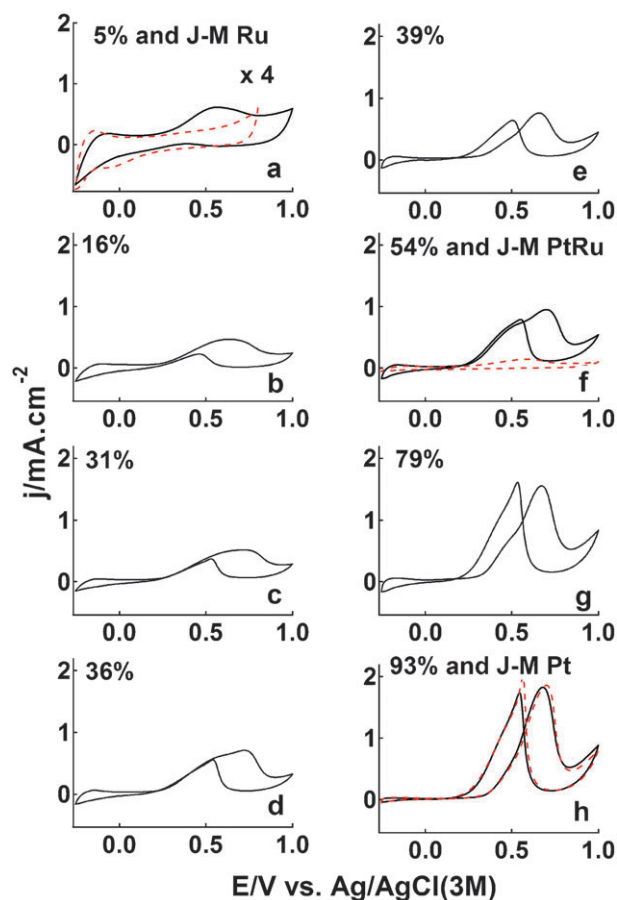


Fig. 6 The CVs of MeOH electro-oxidation on the 8 Pt-decorated Ru samples. The CVs (dashed curves) on the J–M Ru, J–M PtRu (1 : 1) alloy, and J–M Pt NPs are also shown in (a), (f), and (h), respectively for the purpose of comparison.

3.2 MeOH electro-oxidation

Fig. 6 presents the MeOH electro-oxidation CVs of the 8 1st-batch and the reference samples. Those of the 3 2nd-batch samples are shown in Fig. S4 in the ESI†. The trend of variation is identical to that in Fig. 6. For the J–M Ru, no MeOH electro-oxidation activity was observed (dashed CV in Fig. 6a) which was in agreement with previous observations,²³ although a recent surface enhanced Raman scattering study by Zou *et al.*⁴⁷ suggested that Ru NPs may have observable MeOH activity at room temperature. However, a deposition of a merely 5% of Pt already initiated small but observable MeOH activity (Fig. 6a). This is in clear contrast to the Pt deposited on a polycrystalline Au substrate on which no MeOH activity was observed at a coverage as high as 22%.²³ This may be rationalized by the difference in Pt–Au and Pt–Ru interactions: Pt solute has a very strong tendency to segregate in a Ru host but a strong tendency towards anti-segregation in a Au host.³⁸ This difference led the Pt to form a segregated Pt adlayer phase (islands) on Ru during the EG reduction period that satisfied the ensemble requirement for the MeOH EO.²³

With the increase of the Pt PD, the transient peak current density of MeOH EO increased and there was a remarkably linear relationship between them as shown in Fig. 5(b) ($y = ax$ with $R^2 = 0.98$). This linear relationship is a strong indication that all deposited Pt atoms were grouped in the form of surface islands since insulated Pt atoms would not be active for MeOH EO. As the Pt PD increased, the pattern of the CV became more and more similar to that of the pure J–M Pt NPs: they almost overlapped at the Pt PD of 0.93 (Fig. 6(h)). This resemblance again indicates that the electronic effect of the Ru substrate became weaker at higher Pt coverages, *i.e.*, the atoms in the Pt adlayer supported by Ru NPs acted more like pure Pt atoms rather than those alloyed to the Ru, as already pointed out in the above discussions of the XRD results. This observation is further substantiated by the striking difference observed between the CV of the Pt(54)–Ru and that of the J–M PtRu (1 : 1) alloy NPs (Fig. 6f). The latter resembled more that of the Pt(5)–Ru (Fig. 6a). Considering that a nominally 45% Pt is expected on the surface of the PtRu alloy NPs, these observations are somewhat unexpected. Two reasons may account for the observations: One is a high segregation of the Ru on the surface of the alloy NPs as recently observed by ¹⁹⁵Pt NMR of PtRu alloy NPs.^{48,49} The other is a solid solution of alloying that resulted in a large part of the Pt sites having insufficient Pt neighbors to form an ensemble needed for MeOH electro-oxidation,²³ *i.e.*, the so-called ensemble effect.⁹

In the real-world DMFC applications, the long-term CO tolerance of electrocatalysts is practically more important than the intrinsic MeOH EO activity as measured by the transient peak current in Fig. 6. In this regard, CA measurements were carried at 0.2 V on the 11 Pt-decorated Ru NP samples to gauge their respective CO tolerance in a 0.5 M MeOH-containing electrolyte solution. The resulting CA curves of the 8 1st-batch samples are shown in Fig. 7A (those of the 3 2nd-batch samples in Fig. S5 in the ESI†). As can be seen, and in agreement with the results presented in Fig. 6 and the extrapolation

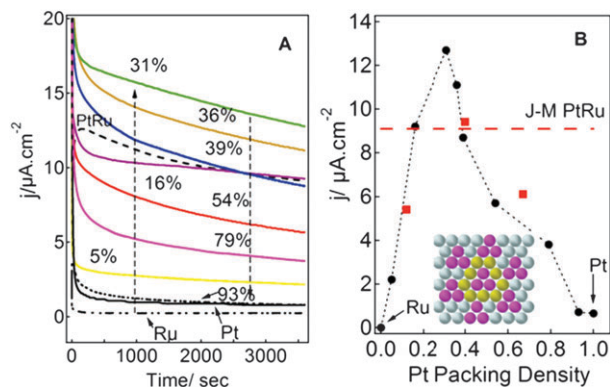


Fig. 7 (A) The CAs of the 8 Pt-decorated Ru NP samples. The CAs of the J–M Ru, J–M PtRu (1 : 1) alloy, and J–M Pt NPs are also shown for the purpose of comparison. (B) The volcano-like curve of CA currents measured at 60 min as a function of the Pt coverage. The inset in (B) is a surface structure model (dark spheres for Pt atoms and light spheres for Ru atoms with each Pt 3-atom ensemble having 9 nearest Ru neighbors) that consists of ensembles of 3 Pt atoms on Ru(0001) and simultaneously has the maximum numbers of Pt ensembles and of Pt/Ru sites. The corresponding Pt PD = $3/7 = 0.43$.

of the straight line in Fig. 5(b) to zero, the J–M Ru NPs did not show any observable MeOH reactivity. On the other hand, the Pt(93)–Ru sample acted almost the same as the pure J–M Pt NPs. However, the J–M PtRu showed a much higher activity (*i.e.* CO tolerance) than both Pt(5)–Ru, Pt(12)–Ru, and Pt(54)–Ru, which seems to be contradictory to the observation gleaned from Fig. 5(a) where higher CO stripping peak potential was observed for J–M PtRu. The exact reason is still unclear at present and warrants further, carefully designed experimental and theoretical investigations.

On the other hand, the CA currents for the 11 Pt-decorated Ru samples closely follow the trend of the CO stripping peak potential as a function of the Pt PD, as shown in Fig. 8. When the CA currents measured at 60 min of the MeOH reaction are plotted as a function of the Pt PD, an expected volcano-like

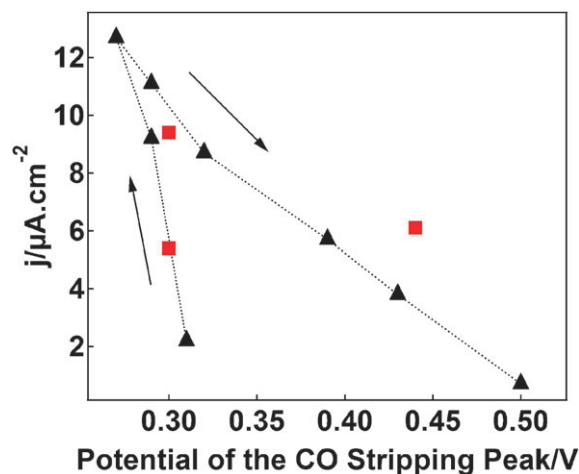


Fig. 8 The correlation between the long-term steady-state current density of the MeOH electro-oxidation and the potential of the CO stripping peak. The squares are for the three second batch samples. The Pt coverage is the implicit parameter in this plot with the arrows indicating the direction of the increasing coverage.

curve as shown in Fig. 7B is observed with the maximum current at the PD of 0.31 that coincides with the lowest CO stripping peak potential (Fig. 8). This volcano curve can be understood as the result of two competing processes in MeOH EO on a Pt-decorated Ru NP surface: the triple dehydrogenation reaction steps being facilitated by the increased Pt ensemble sites that would lead to the generation of more poisonous CO and the enhanced CO eliminating ability through the bifunctional mechanism offered by the presence of more adjacent Ru/Pt sites as well as the possible synergistic electronic (ligand and strain) effect at the lower Pt PDs that weakens the Pt–CO bonding.^{38–40} As the Pt PD increased but before the volcano peak, the two processes could work in unison because both the dehydrogenating ensemble sites and the CO-eliminating ability increased (the latter is indicated by the continuous negative shift of the CO stripping peak potential), and so did the reaction current. Beyond the volcano peak, although a further increase in Pt coverage would increase the dehydrogenating ensemble sites, the accompanying decrease in the CO-eliminating ability, as indicated by the positive shift of the CO stripping peak potential (Fig. 5 and 8), led to the decrease of the overall current. The difference in slope before and after the volcano peak as shown in Fig. 8 may be indicative of the difference in electronic effect⁵⁰ of the Ru substrate which appeared to be stronger at lower Pt PDs. Overall, one can conclude that the Pt(31)–Ru sample had the optimal compromising surface structure/electronic effect that maximized the overall reaction current. This should be compared to the Ru-decorated Pt NPs where the maximum activity appeared at 40 to 50% of Ru packing density.¹⁹ Most remarkably, the Pt(31)–Ru sample showed an impressively high reactivity that was about 150% higher than that of the industrial benchmark J–M PtRu (1 : 1) alloy sample but with at least 3.5× less Pt loading. It is also worth noting that the Pt(16), Pt(36), and Pt(39)/(40)–Ru samples all showed either higher or comparable MeOH long-term activity as compared to that of the J–M PtRu (1 : 1) alloy sample but with lower Pt loadings.

4. Conclusions

In conclusion, we have reported the development of a superior, industrially scalable one-pot EG based wet chemistry method to prepare Pt-decorated Ru NPs that offers an exquisite control of the Pt PD of the Pt adlayers with, most likely, mono-atomic height and effectively prevents the NPs sintering during the deposition. Using the 3 nm J–M Ru NPs as the starting material, 11 samples with different Pt PD ranging from 0.05 to 0.93 were prepared, characterized, and studied in detail for the MeOH EO. A volcano curve in terms of long-term activity as a function of the Pt coverage was observed and peaked at the Pt PD of 0.31, attesting the competition of the two processes that are both essential for the MeOH EO: the triple dehydrogenation and the elimination of poisonous CO. An increase of the Pt ensemble sites will facilitate the former *via* the ensemble effect while an increase of the adjacent Ru/Pt sites will enhance the latter *via* the bifunctional mechanism. Assuming an ensemble of minimum three Pt atoms is needed for EO of MeOH,

the surface structure shown in the inset of Fig. 7(B) gives, simultaneously, the maximum numbers of ensembles and of Pt/Ru sites on a Ru(0001) surface. The corresponding Pt PD is $3/7 = 0.43$, reasonably close to the Pt PD (0.31) of the most active sample. Notice that Gasteiger *et al.* did a statistical analysis of a Pt–Ru alloy surface using a model of a 3 Pt atoms ensemble that had only one Ru atom as the nearest neighbor and found out the optimal Pt content was about 88%.¹⁰ Thus, this simple analysis suggests that on Ru@Pt, more than one Pt/Ru site per Pt ensemble is needed to achieve the highest activity.

Additionally, the CO eliminating ability might also be enhanced at the lower Pt PDs by the electronic effect.^{38–40,50} The direct correlation between the long-term steady-state MeOH EO current density and the CO stripping peak potential highlights again the technological importance of optimizing this CO-eliminating ability. However, evidence suggested that, for the higher Pt PD adlayers formed on the Ru NP surface, electronic effects exerted by the Ru substrate were very weak, if at all. This is in contrast to the theoretical calculations^{38,40,50} and warrants further scrutiny. Nonetheless, and most significantly, the reactivity of the Pt(31)–Ru sample was about 150% higher than that of the industrial benchmark J–M PtRu (1 : 1) alloy sample but with 3.5 times less Pt loading. The specific activity we obtained is generally higher than or at least comparable to those¹⁸ of the systems made by spontaneous depositions *via* repetitive hydrogen reductions. Considering that Ru is currently about seven times less expensive than Pt, using the Pt(31)–Ru NPs would lower the electrode material cost by more than 50% compared to using the industrial benchmark J–M PtRu (1 : 1) alloy NPs for DMFC applications. Furthermore, the wet chemistry based EG method for the controlled deposition of submonolayer Pt is advantageous in terms of processing and maximizing the use of Pt and can, in principle, be scaled up straightforwardly to an industrial level.

Acknowledgements

B.D. and YY.T. gratefully acknowledge the financial support from DOE (DE-FG02-07ER15895) and thank Ms O. Zaluzhna for taking TEM pictures shown in Fig. S3 and S4 (ESI†), Professor K. T. Holman for discussions on the XRD results, and Mr O. Ugono and Ms S. Kumalah for assistance in the XRD measurements. We acknowledge the support of the Maryland NanoCenter and its NispLab. The NispLab is supported in part by the NSF as a MRSEC Shared Experimental Facility.

DISCLAIMER: Certain commercial equipment, instruments, or materials are identified in this paper in order to specify the experimental procedure. Such identification is neither intended to imply recommendation or endorsement by the National Institute of Standards and Technology nor is it intended to imply that the materials or equipment identified are necessarily the best available for the purpose for which they were used.

References

- 1 M. S. Wilson and S. Gottesfeld, *J. Appl. Electrochem.*, 1992, **22**, 1–7.
- 2 Z. Jusys, J. Kaiser and R. J. Behm, *Langmuir*, 2003, **19**, 6759–6769.
- 3 A. N. Gavrilov, E. R. Savinova, P. A. Simonov, V. I. Zaikovskii, S. V. Cherepanova, G. A. Tsirlina and V. N. Parmon, *Phys. Chem. Chem. Phys.*, 2007, **9**, 5476.
- 4 C. Lu, C. Rice, R. I. Masel, P. K. Babu, P. Waszczuk, H. S. Kim, E. Oldfield and A. Wieckowski, *J. Phys. Chem. B*, 2002, **106**, 9581–9589.
- 5 K. W. Park, J. H. Choi, B. K. Kwon, S. A. Lee, Y. E. Sung, H. Y. Ha, S. A. Hong, H. Kim and A. Wieckowski, *J. Phys. Chem. B*, 2002, **106**, 1869–1877.
- 6 A. O. Neto, R. R. Dias, M. M. Tusi, M. Linardi and E. V. Spinace, *J. Power Sources*, 2007, **166**, 87–91.
- 7 J. A. Tian, G. Q. Sun, L. H. Jiang, S. Y. Yan, Q. Mao and Q. Xin, *Electrochem. Commun.*, 2007, **9**, 563–568.
- 8 M. P. H. Hogarth and G. A., *Platinum Met. Rev.*, 1996, **40**, 150.
- 9 A. Hamnett, *Catal. Today*, 1997, **38**, 445–457.
- 10 H. A. Gasteiger, N. Markovic, P. N. Ross and E. J. Cairns, *J. Phys. Chem.*, 1993, **97**, 12020–12029.
- 11 S. Rojas, F. J. Garcia-Garcia, S. Jaras, M. V. Martinez-Huerta, J. L. G. Fierro and M. Boutonnet, *Appl. Catal., A*, 2005, **285**, 24.
- 12 M. Inoue, H. Shingen, T. Kitami, S. Akamaru, A. Taguchi, Y. Kawamoto, A. Tada, K. Ohtawa, K. Ohba, M. Matsuyama, K. Watanabe, I. Tsubone and T. Abe, *J. Phys. Chem. C*, 2008, **112**, 1479.
- 13 G. S. Chai, S. B. Yoon, J. H. Kim and J. S. Yu, *Chem. Commun.*, 2004, 2766–2767.
- 14 K. Han, J. Lee and H. Kim, *Electrochim. Acta*, 2006, **52**, 1697–1702.
- 15 N. Jha, A. L. M. Reddy, M. M. Shaijumon, N. Rajalakshmi and S. Ramaprabhu, *Int. J. Hydrogen Energy*, 2008, **33**, 427–433.
- 16 S. R. Brankovic, J. X. Wang and R. R. Adzic, *Electrochem. Solid-State Lett.*, 2001, **4**, A217.
- 17 W. Chrzanowski and A. Wieckowski, *Langmuir*, 1997, **13**, 5974–5978.
- 18 S. T. Kuk and A. Wieckowski, *J. Power Sources*, 2005, **141**, 1–7.
- 19 P. Waszczuk, J. Solla-Gullon, H. S. Kim, Y. Y. Tong, V. Montiel, A. Aldaz and A. Wieckowski, *J. Catal.*, 2001, **203**, 1–6.
- 20 M. M. Watanabe and S., *J. Electroanal. Chem.*, 1975, **60**, 267.
- 21 V. Le Rhun, E. Garnier, S. Pronier and N. Alonso-Vante, *Electrochem. Commun.*, 2000, **2**, 475–479.
- 22 W. Vogel, V. Le Rhun, E. Garnier and N. Alonso-Vante, *J. Phys. Chem. B*, 2001, **105**, 5238–5243.
- 23 B. C. Du and Y. Y. Tong, *J. Phys. Chem. B*, 2005, **109**, 17775–17780.
- 24 J. M. B. Wang, S. R. Zhu, Y. Hanson, J. C. Adzic and R. R., *J. Electrochem. Soc.*, 2003, **150**, A1108.
- 25 S. R. Brankovic, J. X. Wang, Y. Zhu, R. Sabatini, J. McBreen and R. R. Adzic, *J. Electroanal. Chem.*, 2002, **524–525**, 231.
- 26 C. L. Green and A. Kucernak, *J. Phys. Chem. B*, 2002, **106**, 1036–1047.
- 27 P. C. Biswas, Y. Nodasaka and M. Enyo, *J. Appl. Electrochem.*, 1996, **26**, 30–35.
- 28 E. C. Herrero, W. Wieckowski and A., *J. Phys. Chem.*, 1995, **99**, 10423.
- 29 A. Sun, J. Franc and D. D. Macdonald, *J. Electrochem. Soc.*, 2006, **153**, B260–B277.
- 30 H. A. C. Kozłowska, B. E. Sharp and W. B. A., *J. Electroanal. Chem.*, 1973, **43**, 9.
- 31 R. E. Benfield, *J. Chem. Soc., Faraday Trans.*, 1992, **88**, 1107.
- 32 S. Alayoglu, A. U. Nilekar, M. Mavrikakis and B. Eichhorn, *Nat. Mater.*, 2008, **7**, 333–338.
- 33 H. A. Gasteiger, P. N. Ross and E. J. Cairns, *Surf. Sci.*, 1993, **293**, 67–80.
- 34 J. W. Guo, T. S. Zhao, J. Prabhuram, R. Chen and C. W. Wong, *Electrochim. Acta*, 2005, **51**, 754–763.
- 35 J. Kaiser, L. Colmenares, Z. Jusys, R. Mörtel, H. Bönemann, G. Köhl, H. Modrow, J. Hormes and R. J. Behm, *Fuel Cells*, 2006, **6**, 190–202.
- 36 H. A. Gasteiger, N. M. Markovic and P. N. Ross, *J. Phys. Chem.*, 1995, **99**, 16757–16767.
- 37 M. T. M. Koper, J. J. Lukkien, A. P. J. Jansen and R. A. van Santen, *J. Phys. Chem. B*, 1999, **103**, 5522–5529.
- 38 B. Hammer and J. K. Nørskov, *Adv. Catal.*, 2000, **45**, 71–129.
- 39 Y. Y. Tong, H. S. Kim, P. K. Babu, P. Waszczuk, A. Wieckowski and E. Oldfield, *J. Am. Chem. Soc.*, 2002, **124**, 468–473.
- 40 J. R. Kitchin, J. K. Nørskov, M. A. Barteau and J. G. Chen, *J. Chem. Phys.*, 2004, **120**, 10240.
- 41 F. Maillard, G. Q. Lu, A. Wieckowski and U. Stimming, *J. Phys. Chem. B*, 2005, **109**, 16230–16243.
- 42 C. E. Lee and S. H. Bergens, *J. Phys. Chem. B*, 1998, **102**, 193–199.
- 43 E. M. Crabb, M. K. Ravikumar, D. Thompsett, M. Hurford, A. Rose and A. E. Russell, *Phys. Chem. Chem. Phys.*, 2004, **6**, 1792.
- 44 C. Roth, N. Benker, R. Theissmann, R. J. Nichols and D. J. Schiffrin, *Langmuir*, 2008, **24**, 2191–2199.
- 45 W. Chrzanowski and A. Wieckowski, *Langmuir*, 1998, **14**, 1967–1970.
- 46 K. A. Friedrich, K. P. Geyzers, A. J. Dickinson and U. Stimming, *J. Electroanal. Chem.*, 2002, **524–525**, 261.
- 47 H. Z. Yang, Y. Q. Yang and S. Z. Zou, *J. Phys. Chem. B*, 2006, **110**, 17296–17301.
- 48 A. L. Danberry, B. C. Du, I. S. Park, Y. E. Sung and Y. Y. Tong, *J. Am. Chem. Soc.*, 2007, **129**, 13806.
- 49 B. Du, A. L. Danberry, I. S. Park, Y. E. Sung and Y. Y. Tong, *J. Chem. Phys.*, 2008, **128**, 052311.
- 50 J. Greeley and M. Mavrikakis, *Nat. Mater.*, 2004, **3**, 810–815.